Femtosecond-Laser-Delamination Cavities for Resonant Acousto-Magneto-Plasmonics

Pavel Varlamov,[1] Akira Barros,[1] Aditya Swaminathan,[1] Jan Marx,[2] Andreas Ostendorf,[2] Anna Semisalova,[3] Denys Makarov,[4] Alexey M. Lomonosov,[5] Paolo Vavassori,[6,7] Yannis Laplace,[1] Michele Raynaud,[1] and Vasily V. Temnov[1,*]

[1]*LSI, Ecole Polytechnique, CEA/DRF/IRAMIS, CNRS, Institut Polytechnique de Paris, 91128 Palaiseau, France*
[2]*Applied Laser Technologies, Ruhr University Bochum, Universitätsstraße 150, 44801 Bochum, Germany*
[3]*Faculty of Physics and CENIDE, University of Duisburg-Essen, 47057 Duisburg, Germany*
[4]*Helmholtz-Zentrum Dresden-Rossendorf e.V., Institute of Ion Beam Physics and Materials Research, Bautzner Landstrasse 400, 01328 Dresden, Germany*
[5]*B W Department, Offenburg University of Applied Sciences, 77652 Offenburg, Germany*
[6]*CIC nanoGUNE BRTA, Donostia San Sebastian, 20018 Donostia, Spain*
[7]*IKERBASQUE, Basque Foundation for Science, 48009 Bilbao, Spain*

Received 10 February 2025; accepted 29 August 2025; published 18 September 2025)

Femtosecond lasers are routinely used for inducing local modification, including nanostructuring, and ultrafast laser spectroscopy in solids. However, these studies are often being performed separately making the unveiling of exciting physical properties of laser-fabricated materials out of reach. Here, we present an all-optical platform combining the fabrication of nano to micrometer size single-shot femtosecond-laser-delamination" membranes or cavities of ferromagnetic thin films and multilayers together with their quasi *in situ* characterization using the Abbe-limited interferometric, ultrafast scanning photo-acoustic and magneto-plasmonic microscopies. Ferromagnetic nickel and iron cavities display high-Q acoustic resonances providing access to long-lived ultrahigh frequency coherent phonon modes in the above 100 GHz frequency range. Cavities in cobalt-gold bilayers allow for magnetically controlled surface plasmon resonance experiments in the Otto configuration, which is otherwise very difficult to implement experimentally. Quantitative experimental characterization of functional magnetic cavities, supported by the numerical modeling of all experimental data, opens an avenue to design and fabricate tunable nanoscaled femtosecond-laser-delamination architectures in thin films and multilayers.

DOI: 10.1103/99sl-xxb2

Experimental access to nano and micrometric cavities enclosed by membranes with nanometer thickness is crucial for fundamental studies of electronic materials with curvilinear and 3D geometries [1]. They facilitate fundamental studies of ultrafast dynamics and applications in ferromagnetic thin films targeting the GHz-to-THz frequency range [2] and high-frequency spin dynamics based on plasmonic metasurface resonators with locally enhanced THz magnetic fields [3]. Understanding mechanisms of high-frequency phonon attenuation [4] or resonantly enhanced phonon-magnon interactions [5,6] is particularly advantageous in such nanoscaled membranes. On the other hand, a suspended film of an arbitrary thickness separated by a micrometer large gap from a dielectric substrate represents one of the basic, yet difficult to implement, configurations in plasmonics known as the Otto geometry [7 10]. Sample preparation for the aforementioned investigations represents a significant challenge, and it would be highly desirable to develop faster, cost-efficient technologies. In the past, femtosecond laser nanofabrication techniques demonstrated a fascinating flexibility in producing functional micromechanical devices [11], an approach that we develop in this Letter by exploring the potential of femtosecond laser nanostructuring of thin film materials in the single-shot regime.

Nanostructuring of absorbing thin films by femtosecond laser pulses is accomplished through a sequence of transient phenomena mediated by the nonequilibrium electron and phonon dynamics and triggering the laser-induced melting and resolidification, the acoustic or hydrodynamic motion of the material, or the irreversible removal ablation) of the irradiated film from the substrate [12,13]. Numerous damage or material modification phenomena can be precisely controlled through their threshold laser fluence in J/cm^2), focusing conditions [14], and film thickness [15].

Through systematic studies [16,17] we managed to control the key parameters governing the process and eventually succeeded in achieving a deterministic separation delamination) of the entire film or multilayer from the dielectric substrate creating closed femtosecond-laser-delamination" FLD) cavities [Fig. 1 a)]. The peak laser

*Contact author: vasily.temnov@cnrs.fr

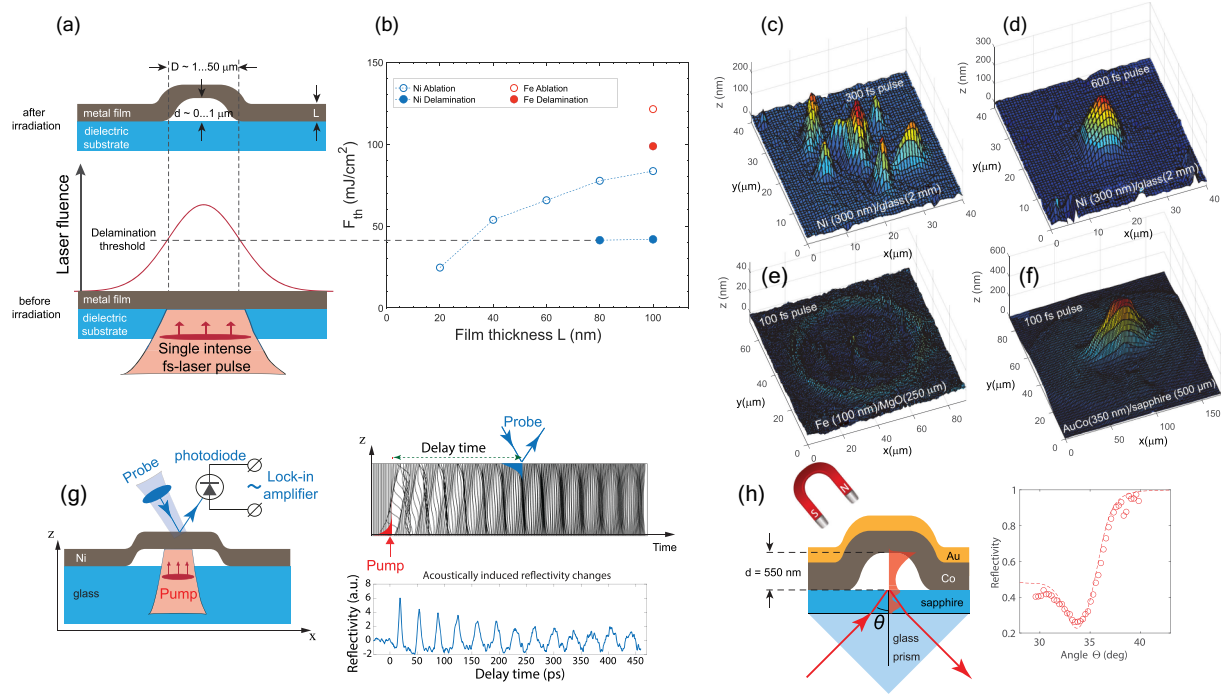

FIG. 1. a) Irradiation of a metallic thin film or multilayer with a single ultrashort laser pulse see Fig. 1S in SM [22]) may create a closed FLD cavity within a certain range of applied laser fluence. b) The delamination fluence strongly depends on the material and the film thickness. c) f) The Abbe-limited interferometric microscopy of irradiated samples delivers different surface morphology depending on the material, thickness of the film and the substrate, and the pulse duration. g) Femtosecond optical excitation of delaminated thin films triggers the long-lived oscillations of coherent acoustic phonons therein probed by time-resolved reflectivity. h) FLD cavities with a sufficiently large separation gap $d \sim$ constitute the Otto configuration for the angular-resolved magneto-)plasmonic studies. The dashed area within the cavity displays the calculated electromagnetic field $H_y(z)^2$ at the resonance angle $\theta = 34°$ in a sapphire substrate and evidences the plasmon excitation at the cobalt-gap interface; see Fig. 5S in SM [22].

fluence must be carefully tuned to exceed the delamination threshold but remain below the thin-film ablation threshold [Fig. 1 b)]. We eventually demonstrated that the deposition of a thin Au layer sandwiched between Ni thin film and glass substrate allowed to achieve significantly smaller ablation and delamination thresholds [17]. Energy balance arguments have been proposed to advocate the dependence of both thresholds on the film thickness L, suggesting that at least a fraction of a femtosecond-laser-excited thin film becomes laser-melted [15,17]. More complex multiparameter models have been developed to evaluate the velocity of the ablating layer [18,19] in the context of the so-called laser-induced forward transfer laser technology, where the ablating material is deposited on a closely spaced substrate [20,21].

The simplistic concept in Fig. 1 a) assumes that the Gaussian distribution of the incident laser fluence is not altered by optical propagation effects in the substrate. However, intense ultrashort laser pulses with a peak power exceeding the critical power of self-focusing are known to suffer from nonlinear Kerr-type) self-focusing effects resulting in the decay of the Gaussian laser beam in multiple filaments [30,31], creating a complex, spatially inhomogeneous distribution of incident laser fluence at a substrate-film interface. An example of a 300 nm thin film on 2 mm glass substrate fingerprints an irregular surface landscape excited by 300 fs laser pulses in Fig. 1 c). Peak power can be lowered and filamentation effects suppressed by using longer 600 fs) laser pulses resulting in formation of deterministic FLD cavities on the same sample [Fig. 1 d)]. FLD cavities produced with 100 fs laser pulses in metallic thin film and multilayer samples deposited on sub-mm thin substrates were deterministic [Figs. 1 e), 1 f)]. However, even in such thin substrates irradiation with sub-100 fs laser pulses generated filaments and white light continuum, advocating the necessity of using longer laser pulses smaller peak powers) to produce deterministic cavities sketched in Fig. 1 a).

In this Letter we show that such quasifreestanding deterministic FLD membranes host a reach physics that can be conveniently addressed via nanophotonic experiments. To characterize these optically produced FLD cavities and their physical properties we have implemented three distinct all-optical microscopic techniques. The Abbe-limited interferometric microscopy [Fig. 2S in Supplemental Material SM) [22]] has been applied to identify and classify different FLD formation regimes [Figs. 1 c) 1 f)]. Femtosecond time-resolved scanning

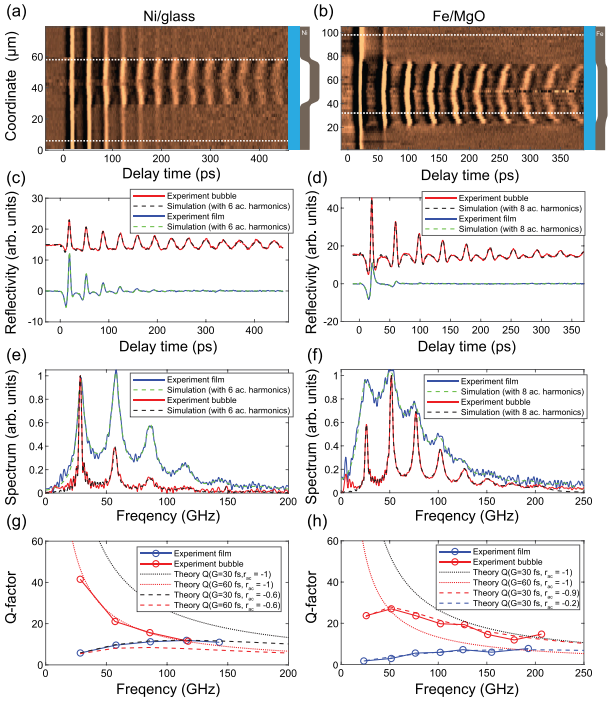

FIG. 2. a), b) Acoustic dynamics across FLD cavities as a function of the pump-probe delay time on Ni/glass and Fe 100)/MgO 100) samples. c), d) The acoustic dynamics on cavities bubbles) are compared with those on unperturbed film and fitted with a superposition of damped acoustic eigenmodes. e), f) Fourier spectra of the dynamics in panels c), d). g), h) Quality factors of individual phonon modes are fitted with the phenomenological Eq. 2) to extract the phonon damping constant G and the acoustic reflectivity r_{ac} of the delaminated interface. Experimental details are given in Sec. IV in SM [22].

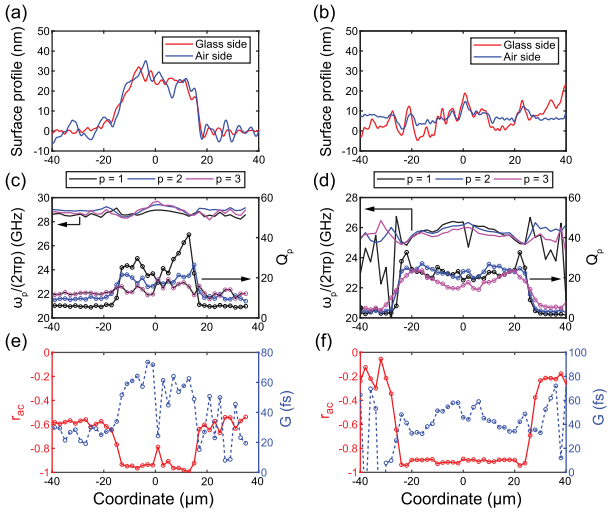

FIG. 3. a), b) Two-sides interferometric microscopy on Ni and Fe cavities. Whereas Ni cavities display measurable gaps $d \simeq 3$ nm, Fe cavities are hardly visible. c), d) Quantitative analysis of the photo-acoustic microscopy: the normalized frequencies $\omega_p/(2\pi p)$ of the first three acoustic harmonics display only a slight variation across the cavity but their Q factors increase within the cavity. e), f) The first four harmonics are fitted with Eq. 1) to map the acoustic attenuation and interface reflectivity, r_{ac}, across the cavity. For both samples the reflectivity value drops below $r_{\mathrm{ac}} <$ .9 getting close to the value of a perfectly reflecting free interface $r_{\mathrm{ac}} =$ 1 confirming the delamination phenomenon. Acoustic attenuation G on FLD shows slight increase as compared to the reference film.

photo-acoustic microscopy [Fig. 1 g) and Fig. 3S] was developed to investigate the dynamics of long-lived acoustic phonon modes generated and confined in FLD cavities. The magneto-plasmonic microscopy in Fig. 1 h) and Fig. 4S has been developed to demonstrate the performance of FLD cavities with larger gaps in the plasmonic Otto configuration [7]. This all-optical platform for single-shot laser nanofabrication and nondestructive quasi *in situ* optical characterization of FLD cavities provides access to upscalable acousto-magneto-plasmonic architectures, including at ultrafast timescales [32].

The optical interferometric microscopy represents the fastest, although extremely precise, approach to the nondestructive quantitative identification of FLD cavities. In case of double-side polished transparent substrates it can be performed from both sides of irradiated thin film. Observing the nearly identical surface landscapes from both sides of the film assures that the delamination of the entire film takes place, without the need to destroy the cavities by performing FIB cross-sectioning and SEM analysis. Throughout this investigation we have analyzed numerous thin films and multilayers and found FLD cavities with separation gaps d ranging from the single digit nanometer in Fe 100 nm)/MgO [see Fig. 1 e) and the discussion of photo-acoustic microscopy in Figs. 2 and 3] to a few hundreds of nanometers and more for much thicker Co/Au bilayers enabling thorough magneto-plasmonic investigations [Fig. 1 f)].

One striking example where FLD micro and nanocavities can show their vast potential both for fundamental studies and for applications is in the investigation of ultrafast photo-acoustics. Thomsen *et al.* [33] demonstrated that the absorption of ultrashort laser pulses by solid thin films and multilayers generate pulses of coherent acoustic phonons, which can be used to study phonon attenuation [34], electron-phonon coupling [35], nonlinear acoustics [36] and nanoscale heat transport [37]. The dominant decay channel of the optically excited oscillations of coherent acoustic phonons in films deposited on a substrate was proven to stem from the acoustic reflection at film-substrate interface. This led to an increasing interest toward experiments in freestanding membranes, which are expected to show a high acoustic reflection coefficient, r_{ac} $r_{\mathrm{ac}} =$ 1 for a perfect solid-vacuum interface). Here, we have developed and applied a scanning photo-acoustic microscopy approach to study the acoustic properties of freestanding membranes as a result of the FLD process.

FLD cavities in 100 nm thin Ni and Fe, identified through optical interferometric) microscopy, were scanned through tightly focused micrometer-sized laser beam to record the dynamics of acoustically induced reflectivity with femtosecond temporal and micrometer spatial resolution [Fig. 1 c)]. Such photo-acoustic microscopy is presented in Figs. 2 a), 2 b) for FLD cavities produced by polycrystalline Ni/glass and crystalline Fe 100)/MgO 100) samples. In both materials femtosecond-laser-induced reflectivity dynamics in a cavity denoted as a bubble) are characterized by exceptionally long-lived acoustic signals as compared to the reference measurements on the substrate denoted as a film); see Figs. 2 c) 2 f). All signals can be accurately fitted in the time domain by superposition of a few damped eigenmodes of acoustic membranes of thickness L with frequencies $\omega_p = c_s(\pi p/L)$ [6], which can be best seen in their Fourier spectra. Jumping ahead to conclusions we found that all observed photo-acoustic dynamics can be fitted with a simple phenomenological model for effective phonon damping, γ_p, for each phonon mode,

$$\gamma_p(\omega_p) = G\omega_p^2 + \frac{c_s}{2L}\ln\frac{1}{r_{\mathrm{ac}}} \tag{1}$$

where the first term accounts for the intrinsic phonon damping in the material and the second term accounts for the effective phonon damping due to the presence of an imperfect interface with a reflection coefficient $r_{\mathrm{ac}} < 1$. The latter may be due to diffuse phonon scattering at a rough interface [37] or finite acoustic transmission from the film to the substrate [38]. The final quantity of interest is the quality Q factor,

$$Q_p = \frac{\omega_p}{2\gamma_p} = \frac{\omega_p}{2G\omega_p^2 + \frac{c_s}{L}\ln\frac{1}{r_{\mathrm{ac}}}} \tag{2}$$

for all acoustic harmonics compared in Figs. 2 g), 2 h). The maximum Q factors, $\simeq 4$ for Ni and $\simeq 3$ for Fe, exceed the respective magnon quality factors $[= 1/(2\alpha)$, where α denotes Gilbert damping] making these structures suitable for studying resonantly enhanced phonon-magnon interactions [6,39].

Using the methodology illustrated in Fig. 2 on two representative pump-probe traces i.e., film and bubble), we have fitted all signals in Figs. 2 a), 2 b) to obtain the acoustic reflectivity r_{ac} and attenuation G across FLD cavities. These results are shown in Fig. 3. Interferometric measurements for Ni [Fig. 3 a)] and Fe [Fig. 3 b)] from the air and glass sides demonstrate that Ni cavities possess a well-defined gap $d \simeq 3$ nm, but in Fe they are hardly measurable. A detailed analysis of interferometric measurements on laser-irradiated surfaces [23] show that tiny phase shifts equivalent to below ~ 1 nm surface displacement are very difficult to discriminate due to the laser-induced modification of the refractive index. However, the formation of FLD cavities in Fe cannot be unequivocally and precisely determined by scanning photo-acoustic microscopy. The frequencies of the first three acoustic eigenmodes in Figs. 3 c), 3 d) show minor variations across the cavity suggesting that the film thickness remained approximately constant. Acoustic quality factors in the same panels demonstrate the pronounced jump with much larger values within FLD cavities in both materials. Fitting the Q factors of the first few acoustic modes with Eq. 2) results in the mapping of acoustic reflectivity r_{ac} and damping G shown in Figs. 3 e), 3 f). A dramatic decrease in surface acoustic reflectivity was observed in both samples—down to the perfect value of $r_{\mathrm{ac}} = 1$ for Ni and $r_{\mathrm{ac}} = .9\ldots .95$ for Fe. This result demonstrates that photo-acoustic microscopy allows for the quantitative identification of FLD formation even in the case of a negligibly small gap d when the vertical resolution of optical interferometry is not sufficient to evidence the delamination phenomenon. A slight increase in the acoustic attenuation parameter G is observed in both materials; its value is consistent with the longitudinal phonon attenuation measured at 9.3 GHz using high-frequency electronic techniques [40]. Our photo-acoustic microscopy on FLD membranes extends the frequency limit to study acoustic phenomena in metals up to 200 GHz, which otherwise requires sophisticated preparation techniques for ultrathin freestanding membranes [4]. Therefore, beyond enabling ultraprecise identification and metrology of FLD micro and nano membranes our results demonstrate their performance in ultrafast quantitative photo-acoustics.

Micron-sized FLD cavities with a gap size of the order of a few hundreds of nanometers offer new opportunities for plasmonics and magneto-plasmonics. We have produced FLD cavities using a Au 100 nm)/Co 250 nm)/sapphire bilayer structure. Interferometric microscopy demonstrates the maximum gap size of 550 nm in the center of the cavity, making the cavity an ideal candidate to implement plasmonics and magneto-plasmonics in the Otto configuration [7,10]. We have mounted the sample on a glass prism and performed spatially resolved reflectivity measurements at different angles of incidence using a tightly focused p-polarized beam of a He:Ne laser at 632.8 nm. As expected, we observe a strong variation of the reflectivity in the center of the bubble; see Figs. 4 a) 4 c).

Angular-dependent reflectivity in the center of the bubble [Fig. 4 d)] displays a clear minimum corresponding to the condition of surface plasmon polariton) resonance SPR), i.e., 34° angle of incidence in the sapphire substrate. Being in agreement with the results of transfer-matrix calculations, this behavior contrasts to a smooth featureless angular dependence of reflectivity from the Co-sapphire interface. For detailed investigation of the magneto-plasmonic properties of FLD cavities, we have implemented the magneto-plasmonic microscopy setup with a kHz-frequency magnetic field that switches the magnetization in the sample plane [24]. The recorded transverse

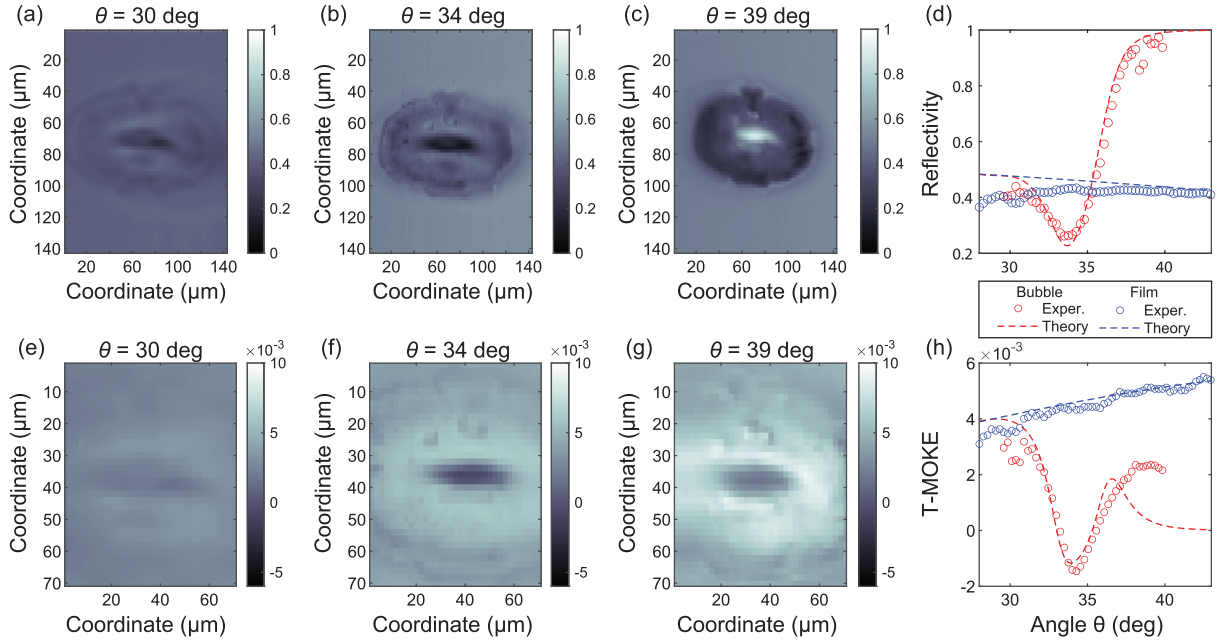

FIG. 4. a) c) Reflectivity maps on a Au/Co/gap/sapphire FLD cavity in Figs. 1 f), 1 h) with a large gap $d = 55$ nm display the strong angular dependence of optical signal in the center of the cavity; the angle of incidence θ is in sapphire. d) The angular dependence of the reflectivity displays a pronounced dip at $\theta = 34°$, which corresponds to the surface plasmon polariton SPP) resonance for the Otto configuration sapphire-gap-cobalt) and is accurately reproduced by the transfer-matrix calculations. The excitation of the SPP resonance at this angle is evident when comparing with a smooth featureless dependence at the unperturbed Co-sapphire interface $d =$, denoted as film). e) g) The transverse magneto-optical Kerr effect T-MOKE) maps for the same three angles θ also show a strong angular dependence. h) Angular dependence of the T-MOKE in the cavity and in the film clearly showing the strong modulation across the SPP resonance, in a good agreement with the magneto-optical transfer-matrix calculations [41]. Experimental details are given in Sec. V in SM [22].

magneto-optical Kerr T-MOKE) signal across the FLD cavity with a $d = 55$ nm gap shown in Figs. 4 e) 4 g) results in a pronounced modulation due to the excitation of the SPP resonance [Fig. 4 h)], in a good agreement with transfer matrix simulations. Extended transfer matrix simulations showed that a tiny modulation of the gap size $d \sim 1$ nm $d/d \sim 1$ ^{3}) would result in a pronounced reflectivity modulation in the vicinity of the SPR with a comparable magnitude as in Fig. 4 h).

Discussion and outlook Beyond the examples readily discussed, the potential of freestanding membranes for nonlinear acoustics at the nanoscale [42,43], including the use of complex materials with structural phase transitions [44], curvilinear magnetism [45,46], and 3D magnonics [47,48], can be further explored. As the fabrication method is not limited to magnetic materials only, it can be applied to different families of electronic materials with nanoscale curved geometries [1], e.g., can act as curvature templates for modifying transport properties in 2D materials [49].

Plasmonic and magneto-plasmonic properties of FLD cavities can open new opportunities for sensing, with an evident idea of using the high sensitivity of the SPR in the Otto configuration to the gap size d for pressure sensing. The combination of our all-optical manufacturing and interrogation approach would allow the development of individual or array nano and micro sensors on a chip capable of detecting minute local changes of pressure in various environments. Being affected by the magnetic field, magneto-plasmonic FLD cavities or their arrays could also offer interesting prospects for precise magnetic field detection. When combined with magneto-elastic excitation mechanisms [39,50], these structures could help exploit extended functionalities offered by ultrafast acousto-magneto-plasmonics [32]. Although the experimental techniques in this Letter were tested on planar 1D structures with $D \gg d$, they are of particular importance to characterize the performance of miniaturized curved architectures with $D \sim$ $\sim 1 \ldots 1$ d, provided by tight focusing conditions. Indeed, the dynamic modulation of the gap size d in the MHz-to-GHz frequency range can be achieved through excitation of flexural acoustic lateral eigenmodes of freestanding membranes with $D \sim$ [16]. Exploring functionality of FLD structures in terms of optical cavities could be also a quite interesting candidate to control quantum-optical properties of light emitters integrated therein [51 54], thin film photovoltaics [55], and ceramic materials [56].

Acknowledgments This work was supported by the ANR-21-MRS1-0015-01 IRON-MAG," the Alexander von Humboldt Foundation, the German Academic

Exchange Service DAAD), the Physics Department of École Polytechnique and Institut Polytechnique de Paris within the framework of a *Projet de Recherche en Laboratoire*, the Newport Corporation, the Spanish Ministry of Science and Innovation under the Maria de Maeztu Units of Excellence Program Grant No. CEX2020-001038-M) and Project No. PID2021-123943NB-I00 OPTOMETAMAG), ERC grant 3DmultiFerro Project No. 101141331). We thank Rainer Kaltofen and Bernd Scheumann HZDR) for the support with preparation of Co/Au samples; Ralf Nett, Michael Niesen, and Christian Hiltner RUB Bochum); Artem Levchuk and Charlie Massé LSI, École Polytechnique) for technical assistance; Nadezhda Shchedrina ICMMO, Université Paris-Saclay) for assistance with figure design.

Data availability The data that support the findings of this article are not publicly available upon publication because it is not technically feasible and/or the cost of preparing, depositing, and hosting the data would be prohibitive within the terms of this research project. The data are available from the authors upon reasonable request.

[1] P. Gentile, M. Cuoco, O. M. Volkov, Z.-J. Ying, I. J. Vera-Marun, D. Makarov, and C. Ortix, Nat. Electron. **5**, 551 2022).
[2] C. Davies, F. Fennema, A. Tsukamoto, I. Razdolski, A. Kimel, and A. Kirilyuk, Nature London) **628**, 540 2024).
[3] L. Tesi, D. Bloos, M. Hrton, A. Beneš, M. Hentschel, M. Kern, A. Leavesley, R. Hillenbrand, V. Krápek, T. ikola *et al.*, Small Methods **5**, 2100376 2021).
[4] J. Cuffe, O. Ristow, E. Chávez, A. Shchepetov, P.-O. Chapuis, F. Alzina, M. Hettich, M. Prunnila, J. Ahopelto, T. Dekorsy *et al.*, Phys. Rev. Lett. **110**, 095503 2013).
[5] J.-W. Kim and J.-Y. Bigot, Phys. Rev. B **95**, 144422 2017).
[6] A. Ghita, T.-G. Mocioi, A. M. Lomonosov, J. Kim, O. Kovalenko, P. Vavassori, and V. V. Temnov, Phys. Rev. B **107**, 134419 2023).
[7] A. Otto, Z. Phys. A **216**, 398 1968).
[8] P. Berini, Adv. Opt. Photonics **1**, 484 2009).
[9] J. Heckmann, K. Pufahl, P. Franz, N. B. Grosse, X. Li, and U. Woggon, Phys. Rev. B **98**, 115415 2018).
[10] E. J. Patiño, L. P. Quiroga S, and C. A. Herreño-Fierro, Plasmonics **18**, 719 2023).
[11] S. Kawata, H.-B. Sun, T. Tanaka, and K. Takada, Nature London) **412**, 697 2001).
[12] K. Sokolowski-Tinten, J. Bialkowski, A. Cavalleri, D. von der Linde, A. Oparin, J. Meyer-ter Vehn, and S. I. Anisimov, Phys. Rev. Lett. **81**, 224 1998).
[13] J. Bonse and J. Krüger, Appl. Phys. A **129**, 14 2023).
[14] F. Korte, J. Serbin, J. Koch, A. Egbert, C. Fallnich, A. Ostendorf, and B. Chichkov, Appl. Phys. A **77**, 229 2003).
[15] M. Domke, L. Nobile, S. Rapp, S. Eiselen, J. Sotrop, H. P. Huber, and M. Schmidt, Phys. Procedia **56**, 1007 2014).
[16] V. V. Temnov, A. Alekhin, A. Samokhvalov, D. S. Ivanov, A. Lomonosov, P. Vavassori, E. Modin, and V. P. Veiko, Nano Lett. **20**, 7912 2020).
[17] P. Varlamov, J. Marx, Y. U. Elgueta, A. Ostendorf, J.-W. Kim, P. Vavassori, and V. V. Temnov, Nanomaterials **14**, 1488 2024).
[18] S. G. Koulikov and D. D. Dlott, J. Photochem. Photobiol. A **145**, 183 2001).
[19] J. Shaw-Stewart, T. Lippert, M. Nagel, F. Nüesch, and A. Wokaun, Appl. Surf. Sci. **258**, 9309 2012).
[20] A. I. Kuznetsov, C. Unger, J. Koch, and B. N. Chichkov, Appl. Phys. A **106**, 479 2012).
[21] P. Delaporte and A.-P. Alloncle, Opt. Laser Technol. **78**, 33 2016).
[22] See Supplemental Material at http://link.aps.org/supplemental/10.1103/99sl-xxb2 for details of thin films deposition and laser nanostructuring, description of experimental setups and solution of Maxwell equations in the Otto configuration, and supporting figures, which includes Refs. [16,23 29].
[23] V. V. Temnov, K. Sokolowski-Tinten, P. Zhou, and D. von der Linde, J. Opt. Soc. Am. B **23**, 1954 2006).
[24] V. V. Temnov, G. Armelles, U. Woggon, D. Guzatov, A. Cebollada, A. Garcia-Martin, J.-M. Garcia-Martin, T. Thomay, A. Leitenstorfer, and R. Bratschitsch, Nat. Photonics **4**, 107 2010).
[25] V. P. Linnik, Dokl. Akad. Nauk SSSR **1**, 18 1933).
[26] E. Cuche, P. Marquet, and C. Depeursinge, Appl. Opt. **38**, 6994 1999).
[27] C. Roddier and F. Roddier, Appl. Opt. **26**, 1668 1987).
[28] Y. Akimov, Opt. Lett. **43**, 1195 2018).
[29] P. Varlamov, A. Barros, A. Swaminathan, A. Lomonosov, M. Raynaud, and V. V. Temnov, Opt. Lett. **50**, 109 2025).
[30] A. Couairon and A. Mysyrowicz, Phys. Rep. **441**, 47 2007).
[31] T. Yan and L. Ji, Ultrafast Sci. **3**, 0023 2023).
[32] V. V. Temnov, Nat. Photonics **6**, 728 2012).
[33] C. Thomsen, H. T. Grahn, H. J. Maris, and J. Tauc, Phys. Rev. B **34**, 4129 1986).
[34] T. C. Zhu, H. J. Maris, and J. Tauc, Phys. Rev. B **44**, 4281 1991).
[35] T. Saito, O. Matsuda, and O. B. Wright, Phys. Rev. B **67**, 205421 2003).
[36] H.-Y. Hao and H. J. Maris, Phys. Rev. B **64**, 064302 2001).
[37] D. G. Cahill, W. K. Ford, K. E. Goodson, G. D. Mahan, A. Majumdar, H. J. Maris, R. Merlin, and S. R. Phillpot, J. Appl. Phys. **93**, 793 2003).
[38] F. Noll, N. Krauß, V. Gusev, T. Dekorsy, and M. Hettich, Photoacoustics **30**, 100464 2023).
[39] A. Alekhin, A. M. Lomonosov, N. Leo, M. Ludwig, V. S. Vlasov, L. Kotov, A. Leitenstorfer, P. Gaal, P. Vavassori, and V. V. Temnov, Nano Lett. **23**, 9295 2023).
[40] R. Homer, G. Alexandrakis, and G. Dewar, J. Appl. Phys. **61**, 4133 1987).
[41] J. Zak, E. R. Moog, C. Liu, and S. D. Bader, Phys. Rev. B **43**, 6423 1991).
[42] V. V. Temnov, C. Klieber, K. A. Nelson, T. Thomay, V. Knittel, A. Leitenstorfer, D. Makarov, M. Albrecht, and R. Bratschitsch, Nat. Commun. **4**, 1468 2013).
[43] P. J. van Capel, E. Péronne, and J. I. Dijkhuis, Ultrasonics **56**, 36 2015).

[44] I. A. Mogunov, S. Lysenko, A. E. Fedianin, F. E. Fernández, A. Rúa, A. J. Kent, A. V. Akimov, and A. M. Kalashnikova, Nat. Commun. **11**, 1690 2020).

[45] D. Makarov, O. M. Volkov, A. Kákay, O. V. Pylypovskyi, B. Budinská, and O. V. Dobrovolskiy, Adv. Mater. **34**, 2101758 2022).

[46] D. Makarov and D. D. Sheka, *Curvilinear Micromagnetism: From Fundamentals to Applications* Springer Nature, Cham, 2022), Vol. 146.

[47] G. Gubbiotti, *Three-Dimensional Magnonics: Layered, Micro-and Nanostructures* CRC Press, New York, 2019).

[48] A. Barman, G. Gubbiotti, S. Ladak, A. O. Adeyeye, M. Krawczyk, J. Gräfe, C. Adelmann, S. Cotofana, A. Naeemi, V. I. Vasyuchka *et al.*, J. Phys. Condens. Matter **33**, 413001 2021).

[49] S.-C. Ho, C.-H. Chang, Y.-C. Hsieh, S.-T. Lo, B. Huang, T.-H.-Y. Vu, C. Ortix, and T.-M. Chen, Natl. Elec. Rev. **4**, 116 2021).

[50] R. Fabiha, J. Lundquist, S. Majumder, E. Topsakal, A. Barman, and S. Bandyopadhyay, Adv. Sci. **9**, 2104644 2022).

[51] D. Pacifici, H. J. Lezec, and H. A. Atwater, Nat. Photonics **1**, 402 2007).

[52] V. V. Temnov, I. Razdolski, T. Pezeril, D. Makarov, D. Seletskiy, A. Melnikov, and K. A. Nelson, J. Opt. **18**, 093002 2016).

[53] G. Findik, M. Biliroglu, D. Seyitliyev, J. Mendes, A. Barrette, H. Ardekani, L. Lei, Q. Dong, F. So, and K. Gundogdu, Nat. Photonics **15**, 676 2021).

[54] F. Freire-Fernández, J. Cuerda, K. S. Daskalakis, S. Perumbilavil, J.-P. Martikainen, K. Arjas, P. Törmä, and S. van Dijken, Nat. Photonics **16**, 27 2022).

[55] S. Xiao, E. L. Gurevich, and A. Ostendorf, Appl. Phys. A **107**, 333 2012).

[56] F. Kiel, N. M. Bulgakova, A. Ostendorf, and E. L. Gurevich, Phys. Rev. Appl. **11**, 024038 2019).